BENEFITS OF ROBUST PARAMETER ESTIMATION TECHNIQUES IN AN AUTOMATED GEOCODING PROCESSING CHAIN

K.H., Gutjahr [a], K.,Scharrer [b],

[a] Joanneum Research Forschungsgeschaft mbH, Institute of Digital Image Processing, Wastiangasse 6, 8010 Graz, Austria – karlheinz.gutjahr@joanneum.at
[b] Ludwig-Maximilians-University, Department of Earth and Environmental Sciences, Section Geology, Luisenstraße 37, 80333 Munich, Germany - K.Scharrer@iaag.geo.uni-muenchen.de

Commission III, WG III/1

KEY WORDS: Mathematics, Modelling, Rectification, Automation, Volcanoes

ABSTRACT:

Accurate geocoding of Earth observing (EO) satellite imagery is one major prerequisite to monitor the Earth's environment. The quality of the obtained geocoded images depends on the accuracy of the sensor model parameters and the accuracy of the used height information. As for monitoring applications automated image processing chains are desired this paper concentrates on the automatisation of the required measurement ground control points (GCPs). Moreover, several methods to make least squares adjustment a robust estimator are presented. To improve the performance of the robust estimation with respect to the reduction of computational effort and reduction of number of GCPs needed, the use of the median absolute deviation is introduced.
The presented general geocoding workflow and the proposed enhancements are tested using an ENVISAT-ASAR scene of the highly active Neovolcanic Zone of Southern Iceland. This test site, prone to natural hazards like volcanic eruptions and massive glacial torrents is equipped with a network of artificial corner reflectors enabling a detailed verification of the proposed approach.

1. INTRODUCTION

Accurate geocoding of Earth observing (EO) satellite imagery is one major prerequisite to monitor the Earth's environment. On the one hand, multi-temporal or/and multi-sensor analyses are very sensitive to registration errors. On the other hand, only a rigorous geocoding procedure which can model topographic effects and the sensor specific imaging geometry allows the combination of EO data with other information sources like e.g. cadastral information. Therefore only those rectification processes are addressed which are based on mathematical sensor models utilizing additional height information.

The quality of the obtained geocoded images depends on the accuracy of the sensor model parameters (like e.g. position and orientation of sensor) and the accuracy of the used height information. This paper concentrates on the first aspect, namely the refinement of the sensor model parameters. These parameters in general are optimized using ground control point (GCP) measurements and least squares adjustment (LSA) techniques. The commonly used height information sources are digital elevation models (DEMs). A lot of further information about the quality aspects of such DEMs can be found in the web, e.g. (Wise, 2000).

Largely automated image processing chains are required for monitoring or near real-time applications. Therefore, any user interaction, like the time and cost consuming and often inaccurate manual ground control point measurement, should be avoided anyhow. On the other side it is a well known characteristic of LSA techniques that erroneous measurements have a great influence on the results obtained. Thus the parameter refinement based on the provided GCP´s should be capable to detect erroneous point information.

Chapter 2 sketches a general DEM based geocoding workflow. In chapter 3 the proposed enhancements to an automated geocoding processing chain and in chapter 4 the obtained results are presented.

2. AUTOMATED GEOCODING PROCESSING CHAIN

2.1 General geocoding workflow

Figure 1 summarizes a general DEM based geocoding workflow. The processing presented here is more or less straight forward. Automated procedures are marked in green colour whereas interactive or iterative procedures are marked in red.

The processing starts at the left top with the import and preparation of the original EO satellite data. This includes on the one hand the extraction of the image data itself ("Image Raster Data"). Secondly, sensor model parameters ("Orbit & Sensor Parameters") are extracted from the meta information. Depending on the type of the sensor at least three different physical sensor models can be distinguished:

1. Perspective sensors (e.g. frame or digital cameras),
2. Optical line scanners (opto-mechanical or pushbroom) and
3. Synthetic Aperture Radar (SAR) sensors.

For each of these physical models the respective mathematical framework is well established (e.g. Raggam & Almer, 1990). A more recent and generic mathematical model is the use of so-called rational polynomial coefficients (RPCs; Dial & Grodecki, 2002).

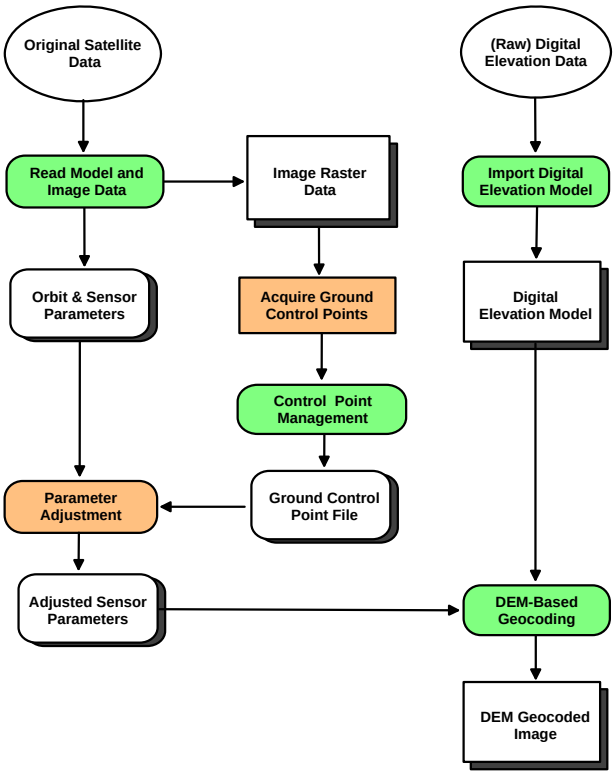

Figure 1. General DEM based geocoding workflow

To achieve optimum rectification accuracy, the sensor model parameters have to be refined in order to achieve "Adjusted Sensor Parameters". This processing step requires ground control point (GCP) measurements. Several proposed approaches to circumvent this interactive task are presented in the next sub section. Basically all methods end up with a list of dedicated points with known ground and image coordinates.

Assuming a sufficient number of GCPs these measurements are then fed into a least squares adjustment (LSA) scheme (Raggam & Almer, 1990, Hellwich & Ebner, 2000, Gutjahr & Raggam, 2000, Dial & Grodecki, 2002).

It is a well known characteristic of LSA that it is very sensitive with respect to erroneous point information. Some so-called robust estimation techniques which try to handle this problem are summarized in the corresponding sub section.

On the right top of Figure 1 the import and preparation of the required DEM is indicated. Finally the optimized sensor parameters and the prepared DEM are used to gecode the satellite image.

2.2 Automated GCP retrieval

Several approaches are presented in literature to circumvent the time and cost consuming and often inaccurate manual ground control point measurement.

The first method uses so-called control point chips (Raggam & Villanueva Fernandez, 2003). These represent small image subsets around manually identified GCPs and are extracted from a reference scene and stored in a database. In every follow-on scene all suitable chips are then identified by applying image matching techniques. Basically this method works for all EO sensor types.

The crucial point is the image matching because the results depend heavily on the similarity of the two images. Secondly, for the reference scene the identification of GCPs has to be done manually at least once.

In case of SAR EO satellites the SAR backscatter can be simulated utilizing an available DEM (Small et. al., 2000). In the simulated SAR image interest points (IPs) can be determined. These IPs can then be found in the real SAR scene again by utilizing image matching techniques. The applicability of this method depends on the quality of the SAR scene and the roughness of the topography of the imaged area.

Alternatively, a very efficient and relatively simple method is the automated detection of corner reflectors (CRs) in SAR scenes (Gutjahr et al., 2005). Of course this method requires the set-up and maintaining of a CR network.

2.3 Robust parameter estimation

In the previous section several methods to automate the GCP acquisition were presented. In any case the parameter refinement based on the provided GCPs should be capable to detect erroneous point information caused by matching or detection errors.

Such techniques are commonly known as robust estimation which means that they are robust with respect to the presence of gross errors in the data. In this context, gross errors are defined as observations which do not fit to the stochastic model of parameter estimation. LSA as mentioned in the previous section is not a robust estimation technique: false observations can lead to completely false results and might even prevent convergence of the adjustment (Rottensteiner, 2001).

The LSA is based on the minimization of the squared sum of the individual residuals v_i:

$$\sum v_i^2 = Min \tag{1}$$

As an alternative to this non robust criterion, the so-called L_2-norm, the minimization of the absolute sum of the residuals, the so-called L_1-norm, can be used

$$\sum |v_i| = Min \tag{2}$$

Adjustment techniques based on this L_1-norm are robust in the above mentioned sense but computationally more complex. Moreover in the presence of pure random errors the performance of the L_2-norm is superior to that of the L_1-norm (Kraus, 1997).

The so-called random sample consensus (RANSAC) algorithm (Fischer & Bolles, 1981) is based on the principle of hypotheses generation and verification. The following steps have to be performed:

1. Choose a minimum set of the GCP measurements.
2. Determine the refined parameters from the minimum set of observations. Thus, the mathematical model must be invertible.
3. Check the other GCPs based on the prediction errors.

4. If the number of accepted GCPs is high enough, then stop, else go to step 1.

The set of GCPs can be chosen randomly. If an estimate for the percentage of gross errors is available in the data, the number of trials required for finding a correct subset of the observations with a pre-defined probability can be estimated. RANSAC is well-suited for problems where the number of parameters is small.

Another way to make the LSA a robust estimator is to eliminate possibly wrong measurements iteratively on the basis of a statistical test. The so-called data snooping (Kraus, 1997) is based on the normalized residuals. Alternatively, the individual residuals can be tested against the overall RMS value of the residuals. In both cases an iterative strategy is applied to determine all erroneous GCP measurements:

1. Find the global solution using all GCP measurements.
2. Test the residuals.
3. Eliminate the measurements which are most likely to be gross errors. Stop if no such observations occur.
4. Determine the global solution omitting all rejected observations and go to step 2.

A last option which should be mentioned here is the so-called Danish method (Krarup et al., 1980). Again it is an iterative solution where the weights of the individual measurements w_i are defined after each LSA step by:

$$w_i = \begin{cases} 1 & |v_i| \le c\,\sigma \\ \alpha \exp(-\beta v_i^2) & |v_i| > c\,\sigma \end{cases} \qquad (3)$$

where σ = a-priori standard deviation of the measurements
α , β = suitable chosen constants
c = multiplication factor determining the probability level (e.g. $c = 2.5$ corresponds to 98.76 percent)

2.4 Robust parameter estimation based on MAD

More or less all methods presented in the previous section may fail if one or more of the following condition is true:

- Only a small number of point measurements is available.
- The number of parameters to be refined is large.
- The percentage of erroneous GCP measurements is high.

Thus a modified version of the Danish method is proposed here which uses the median absolute deviation (MAD) of the point residuals as quality criterion (Huber, 1981). Similar to (3) after each LSA iteration the weights of the measurements are defined by:

$$w_i = \begin{cases} 1 & |v_i| \le c\,s \\ \alpha \exp(-\beta |v_i| s^{-1}) & |v_i| > c\,s \end{cases} \qquad (4)$$

where s = estimation of the standard deviation
α , β and c = analogous to (3)

Here the estimation of the standard deviation based on the MAD according to:

$$\begin{aligned} \tilde{y} &= median(y_i) \\ \mathrm{MAD} &= median\left(|\tilde{y} - y_i|\right) \\ s &= 1.483\,\mathrm{MAD} \end{aligned} \qquad (5)$$

where y_i = individual measurements

The multiplication factor yielding the estimate of the standard deviation from the MAD is the inverse of the normal cumulative distribution function evaluated at the probability level of 75 percent.

3. TESTDATA

3.1 Testsite

Mýrdalsjökull is the fourth largest Icelandic ice cap with an expanse of approx. 590 km² (Jaenicke et al., 2006). It is located at the south coast of the island and the south-eastern end of the highly active Neovolcanic Zone (NVZ). Morphologically the ice cap can be divided into a plateau, where the ice forms a contiguous cover down to about 1300 – 1000 m a.s.l., and the peripheral zone below, where the ice cap splits into separate outlet glaciers.

The glacier ice covers the approximately 100 km² large caldera of the active central volcano Katla that last erupted in 1918. Besides the usual volcanic hazards, the volcano-ice interaction during eruptions leads to enormous melt water torrents, devastating large areas in the surroundings of the glacier.

Considering the eruption cycle of this subglacial volcano (dormant phase max. 80 years, min. 13 years) and the significant increase in seismic activity over the recent years, a fresh outbreak releasing huge glacial torrents is expected in the near future (Larsen, 2000). At the last major event in 1918 the glacier's discharge reached peak rates of 300.000 m³/s (Tómasson, 1996).

Due to this hazardous character Mýrdalsjökull is monitored by SAR remote sensing since 1994. Currently ENVISAT-ASAR acquires data continuously over the test site.

3.2 Image data

The ENVISAT-instrument is a side looking C-band SAR antenna operating at a wavelength of 5.6 cm. Due to its beam steering capability the ASAR instrument can acquire images in seven different swathes (IS1 – IS7), covering an incidence angle range from 15 to 45 degrees. The swathes IS 2 (incidence angle 21.5°) and IS 5 (incidence angle 37.5°) are continuously acquired over the ice cap. This allows the monitoring of the subglacial volcanic activities with a temporal repetition of up to nine days including ascending (asc) and descending (desc) orbits.

In this study an ENVISAT scene acquired on an ascending orbit in the antenna mode IS 2 with vertical transmit-and-receive (VV) polarisation was used. The scene was recorded on 2004-06-20 at about 10:20 p.m. local time.

3.3 Corner reflectors

In view of the upcoming ERS-Tandem mission corner reflectors were set up around the test sites Mýrdalsjökull (Figure 3) and Hekla in 1995 (5 ascending, 5 descending at each site). The third test site Vatnajökull was equipped in 1997.

All CRs are located in areas with low surface roughness. The spatial separation between the reflectors for the ascending and descending satellite passes is 150 m at minimum to avoid interferences of the backscattered signal (Figure 2).

Due to the same orbit constellation of the ERS-1/2 and ENVISAT satellites the CRs can be fully used as ground reference for both missions.

Figure 2. Location of the reflectors M4 at Mýrdalsjökull test site. The CR related to the descending orbit is in the foreground, the ascending CR in the middle ground (red arrow).

4. RESULTS

The proposed automated geocoding processing chain including the automated detection of CRs and the robust parameter estimation based on the MAD was applied to the above mentioned ENVISAT scene. To show the advantages of this approach the same GCPs were used in a LSA scheme where the individual residuals are tested against the overall RMS value of the residuals. Due to the limited number of GCPs only time and range parameters (comprising 4 unknowns) were refined.

Table 1 summarizes the individual image residuals of all detected CRs. The units are in pixels of the single look complex image (SLC). In addition the root mean square error (RMS) and the mean of the individual residuals are shown. Obviously, the CRs M1 and M5 do have a different behaviour than the other 3 CRs which are more or less consistent.

ENV_2004_06_20	Image residuals	
Units: SLC pixels	Azimuth	Range
M1	-29.91	-329.84
M2	-6.07	7.21
M3	-5.98	7.13
M4	-6.04	6.87
M5	-25.80	-204.35
RMS	18.27	173.61
Mean	-14.76	-102.60

Table 1. Initial GCP residuals

If the individual residuals were tested against the overall RMS value of the residuals the automated GCP removal could not detect the erroneous CRs and no GCP was removed automatically. Thus the LSQ converged with zero mean but the RMS values remained high (Table 2).

ENV_2004_06_20	Image residuals	
Units: SLC pixels	Azimuth	Range
M1	-16.59	-96.66
M2	5.02	-124.33
M3	6.14	8.92
M4	12.03	-49.18
M5	-6.59	12.59
RMS	10.26	74.10
Mean	0.00	0.00

Table 2. Adjusted GCP residuals without MAD criterion

The results of the robust LSA by re-weighting the GCP based on the MAD are shown in Table 3.

ENV_2004_06_20	Image residuals	
Units: SLC pixels	Azimuth	Range
M1	-23.88	-337.29
M2	-0.04	-0.03
M3	0.05	0.09
M4	-0.01	-0.06
M5	-19.77	-211.77
RMS	0.04	0.06
Mean	0.00	0.00

Table 3. Adjusted GCP residuals with MAD criterion

According to their large individual residuals the GCPs M1 and M5 were down-weighted and excluded from the RMS and mean calculation. Thus they did not contribute to the final adjustment results. As above the LSA converged with zero mean but with a dramatically better RMS.

5. CONCLUSIONS

In this paper a general geocoding workflow was presented. As largely automated image processing chains are required for monitoring applications, alternatives to the time intensive and often inaccurate manual GCP measurement are described Secondly, several methods to make least squares adjustment a robust estimator were presented. The proposed modifications to the so-called Danish methods yielded dramatically better results than the tested alternative approach.

5. REFERENCES

Dial G., Grodecki J., 2002. Block adjustment with rational polynomial camera models. Proceeding of ASCM-ASPRS Annual Conventions, Washington D.C., April 2002.

Fischler M.A., Bolles R.C., 1981. Random Sample Consensus: A Paradigm for Model Fitting with Applications to Image Analysis and Automated Cartography. Comm. of the ACM, Vol 24, pp 381-395, 1981.

Gutjahr KH., Raggam H., 2000. INSAR Block Parameter Adjustment, Proc. of EUSAR 2000, pp. 493-496, Munich, May 23-25, 2000.

Gutjahr KH., K. Scharrer and U. Münzer, 2005. Utilizing the CR-network in Iceland for an automated interferometric processing chain – Case study with ERS-Tandem data. Proceedings of the Fringe 2005 workshop, 28 Nov. – 2 Dec 2005, Frascati, Italy, published on CD-ROM, available under http://earth.esa.int/workshops/fringe2005/participants/380/paper_Paper_CR_detection.pdf (PDF-format, 6 pages, accessed 10 Apr. 2007).

Hellwich O., Ebner H., 2000. Geocoding SAR-Interferograms by Least Squares Adjustment, ISPRS J. of Photogrammetry and Remote Sensing, 2000, 55(4), pp. 277–288

Huber, P.J., 1981. *Robust statistics*. Wiley, New York, pp. 308.

Jaenicke J., Mayer C., Scharrer K., Münzer U., Gudmundsson Á., 2006. The use of remote sensing data for mass balance studies at Mýrdalsjökull ice cap, Iceland.- J Glaciol, 52, 179, 565-573

Krarup T., Juhl J. and Kubik K., 1980. Götterdämmerung over least squares adjustment. 14th Congress of the Int. Soc. of Photogrammetry, Hamburg, Vol B3: 369-378

Kraus, K., 1997. *Photogrammetry Volume 2. Advanced Methods and Applications*. Dümmler Verlag, Bonn, Germany, fourth edition. pp. 231-234.

Larsen G., 2000. Holocene eruptions within the Katla volcanic system, south Iceland: Characteristics and environmental impact. Jökull 49: 1-28

Raggam H., Villanueva Fernandez M.D., 2003. Approaches to automate image geocoding and registration, Proc. of IEEE Int. Geoscience and Remote Sensing Symposium, Toulouse, 21-25 July 2003, published on CD-ROM

Raggam H., Almer A., 1990. Mathematical Aspects of Multi-Sensor Stereo Mapping. In Proc. of 10'th Annual IGARSS Symposium: Remote Sensing - Science for the Nineties, Vol. III, Seiten 1963-1966.

Rottensteiner F., 2001. Semi-automatic extraction of buildings based on hybrid adjustment using 3D surface models and management of building data in a TIS, PhD thesis submitted to Vienna University of Technology, 2001, available at http://www.ipf.tuwien.ac.at/fr/buildings/diss/dissertation.html (accessed 10 Apr. 2007).

Small D., Biegger S., Nüesch D., 2000. Automated Tiepoint Retrieval through heteromorphic Image Simulation for Spaceborne SAR Sensors, Proc. of ERS-ENVISAT Symposium 2000, ESA Publication SP-461, Gothenburg, Sweden, Oct. 16-20, 2000

Tómasson H., 1996. The Jökulhlaup from Katla in 1918. Annals of Glaciology 22, pp. 249-254

Wise S.M., 2000. Guest editorial: GIS data modelling lessons from the analysis of DTMs. *Int. Journal of Geographical Information Science* 14(4), 313-318, more links available http://www.shef.ac.uk/geography/staff_cms/wise_stephen/dtm/dtm.htm

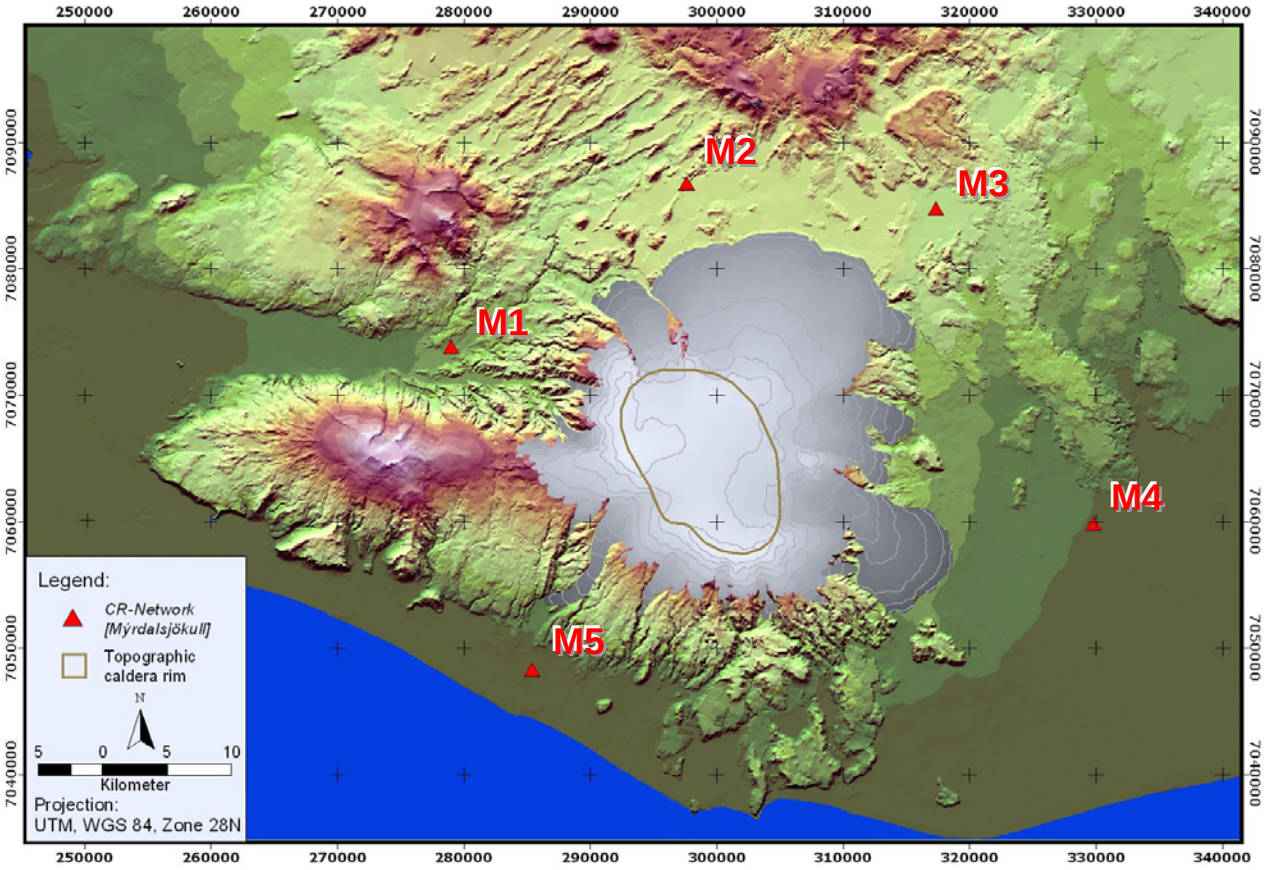

Figure 4. Shaded relief of the Mýrdalsjökull test site with the locations of the corner reflectors.